Journal of Applied Fluid Mechanics , Vol. 9, No. 5, pp. 2321-2332, 2016.
Available online at www.jafmonline.net, ISSN 1735-3572, EISSN 1735-3645.
DOI: 10.18869/acadpub.jafm.68.236.23211

A Note on Bubble Sizes in Subcooled Flow Boiling at Low Velocities in Internal Combustion Engine-Like Conditions

A. J. Torregrosa[1†], A. Broatch[1], P. Olmeda[1] and O. Cornejo[1]

CMT - Motores Térmicos, Universitat Politècnica de València, Aptdo. 22012, E-46071 Valencia, Spain

† *Corresponding Author Email*: *atorreg@mot.upv.es*

(Received May 22, 2014; accepted November 11, 2015)

ABSTRACT

Current trends in engine design indicate the necessity to take advantage of the highest rates of heat transfer associated with nucleate boiling, mostly at high engine loads. When used in conjunction with advanced thermal management strategies, subcooled boiling may take place at very low velocities, for which little information is available, and in ducts with small cross-sectional area, so that undesired effects of the relative sizes of ducts and bubbles may appear. In this paper, experiments on subcooled boiling flow at low velocities and engine-like temperature conditions were conducted with a usual engine coolant. A high-speed photographic camera was used to collect images of the detached vapor bubbles, and the microscopic characteristics of the heating surface were determined. Experimental results for the mean values show acceptable agreement with the results of a mechanistic radius model, when assuming that departure and lift-of radius are related through the flow boiling suppression factor. Additionally, the results obtained are compatible with the sizes of the nucleation sites estimated from the surface characterization. The results obtained for the size distribution are consistent with those found in the literature.

Keywords: Engine cooling; Bubble radius; Bubble size distribution; Heater surface structure.

NOMENCLATURE

b	asphericity factor	r_m	mean radius
$c_{p,f}$	liquid specific heat at constant pressure	Re_b	bubble Reynolds number
C_d	steady drag coefficient	$\mathrm{Re}_{2\phi}$	two-phase Reynolds number
C_r	relative velocity coefficient	S	suppression factor
C_s	wall constant	t_d	departure time
C_{sl}	shear lift coefficient	t_{lo}	lift-off time
F_{bcy}	buoyancy force	t_{sld}	sliding time
F_{du}	bubble growth force	T_i	inlet temperature
F_{sd}	steady drag force	T_m	mean temperature
F_{sl}	shear lift force	T_s	saturation temperature
g	gravitational acceleration	T_w	wall temperature
G_s	dimensionless velocity gradient	u	relative bubble velocity
h_{nb}	nucleate boiling heat transfer coefficient	u^+	non-dimensional velocity profile
Ja	Jacob number	U_f	bulk flow velocity
k	thermal conductivity	y^+	non-dimensional coordinate
l_{fg}	latent heat of vaporization		
p	pressure	α	thermal diffusivity
P	probability density function	μ	dynamic viscosity
q_w	wall specific heat flux	ρ_f	liquid density
q_{fc}	forced convection specific heat flux	ρ_g	vapor density
q_{nb}	nucleate boiling specific heat flux	σ	standard deviation
r	bubble radius	τ_w	wall shear stress
r_d	departure radius	θ	bubble inclination angle
r_{lo}	lift-off radius	ζ	friction factor

1. INTRODUCTION

In current internal combustion engines, fuel consumption and emissions must be reduced without significant penalties in performance (Knecht 2008). One of the preferred solutions for achieving these concurrent requirements is engine downsizing, among other possible solutions (Taylor 2008). However, this technical solution presents a serious heat transfer problem due to the increase in relative heat losses, which may even affect engine durability (Singh *et al.* 2013) and actually poses intrinsic limitations to the reduction of engine size (Sher and Sher 2011). It is therefore justified that advanced cooling systems have regained interest in the engine community (Torregrosa *et al.* 2006; Torregrosa *et al.* 2008).

In this context, nucleate boiling appears to be an interesting option, in view of the high heat transfer rates associated with the process (see, for instance, Sarafraz (2013)). Subcooled boiling flow is particularly attractive for engine cooling system design, because the bubbles collapse in the outer bulk flow region, which therefore contains only liquid phase so that the overall design of the cooling system is substantially unaffected (Steiner *et al.* 2011). However, increased control on magnitudes relevant for heat transfer, as that provided by advanced thermal management strategies (Pang and Brace 2004), is imperative if the the potential benefits of nucleate boiling are to be exploited, mostly at high engine loads.

It is well established (Finlay *et al.* 1985; Ajotikar *et al.* 2010) that nucleate boiling occurs in many engines under conditions within the typical operating range of coolant mass flow rate and temperature. It is important to notice, however, that any lack of control on vapor generation could have catastrophic consequences associated with material overheating (Campbell and Hawley 2003). In this sense, precision cooling appears to provide the best frame for the exploitation of nucleate boiling without excessive risk (Campbell *et al.* 1997; Robinson *et al.* 1999). In that case, a remaining issue to be addressed would be the eventual problems related with the presence of bubbles in the small cross-section ducts characteristic of precision cooling. Therefore, information of typical bubble diameters and their distribution for given operating conditions is required. Additionally, the bubble size distribution and the bubble departure diameter provide important closure relationships for the numerical prediction of subcooled boiling flows (Tu and Yeoh 2002; Torregrosa *et al.* 2015).

Studies on the phenomenon of bubble detachment were initially tackled by Forster and Zuber (1955) and Zuber (1961) in the case of pool boiling. The formation, growth and detachment of bubbles are governed by a number of forces, and from their balance it is possible to determine approximately the diameter of the vapor bubble, as first developed in the case of flow boiling by Zeng *et al.* (1993), considering the balance on the entire bubble, and by Kandlikar and Stumm (1995) considering two separate control volumes for the front and rear regions of the bubble. This force-based approach has been applied to different fluids and flow configurations (Steiner *et al.* 2005; Situ *et al.* 2008; Cho *et al.* 2011; Chen *et al.* 2012). However, a serious difficulty comes from the uncertainties in the expressions for some of the forces governing the size of the vapor bubble as it grows in its nucleation site. Additionally, the experimental determination of bubble diameters is a very complex task and different competing expressions can be found in the literature (Hamzekhani *et al.* 2015).

The wide dispersion in the diameter of the bubbles may be due to an increase in turbulence associated with factors such as coolant temperature fluctuations or hydrodynamic effects (Klausner *et al.* 1997; Mei *et al.* 1995). Of course, the precise characteristics of the heating surface should also play an important role in the development of the process, as demonstrated for instance by Wu *et al.* (2008).

The objective of this paper is to provide additional evidence on the characteristics of bubble size distributions in a usual engine coolant (a mixture of 50% water and 50% ethylene glycol) at low velocities representative of those expected when advanced engine cooling concepts are used, and in which the effect of boiling may be dominant over that of convection (Lee *et al.* 2013). Experimental estimates of the diameter of the bubbles were obtained from high-speed photographic images for several flow velocities. The analysis was carried out following two main lines: the study of the ability of available mechanistic models for reproducing the mean bubble diameter under certain flow and superheating conditions, and the evaluation of the possibility of complementing those mean values with a suitable estimate of the diameter distribution, so that any issue related with the relative sizes of the bubbles and the cooling passages may be considered.

The paper is organized as follows: First, in Sec-

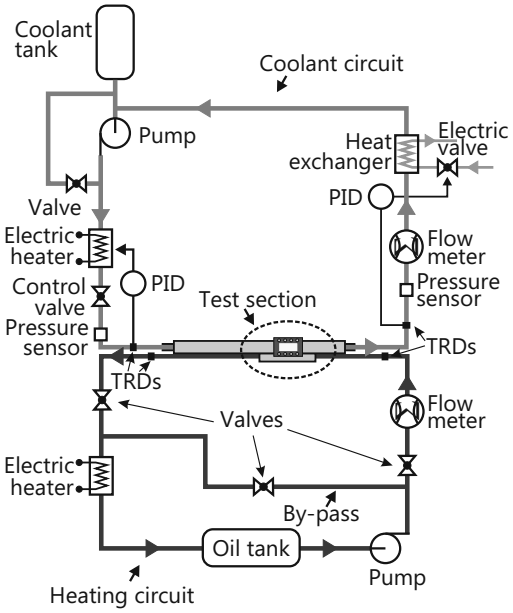

Fig. 1. Schematic of the experimental set-up.

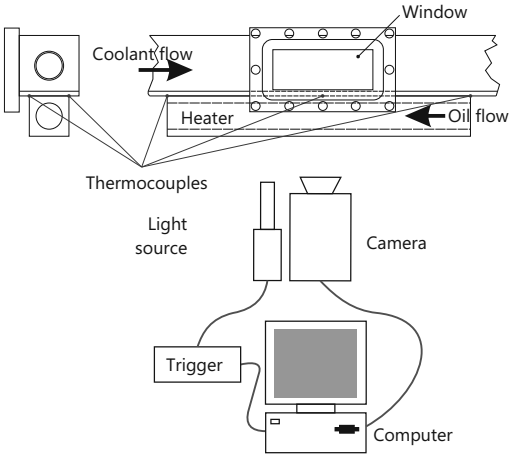

Fig. 2. Test section and instrumentation.

tion 2 the experimental set-up and the instrumentation used are described. Then, in Section 3 the models used for bubble radius prediction are presented, and the estimation of empirical model parameters from the data available is discussed. Section 4 is devoted to the analysis of the results obtained, both in terms of average values and bubble size distributions. Finally, in Section 5 the conclusions of the work are summarized.

2. EXPERIMENTAL SET-UP

A duct was designed so that evaporation could be produced under forced flow conditions comparable to those occurring in cooling systems of internal combustion engines. The system consists of two independent circuits that exchange heat only at the test section. The coolant fluid flows through the first circuit (top of Fig. 1.), which includes a settling tank, a heat exchanger, a liquid pump and an electrical heater, allowing control of both the coolant temperature and volume flow at the inlet of the test section. The volume flow is measured with an electromagnetic flow meter and regulated by manual adjustment of a control valve and of the by-pass valve of the pump. The coolant temperature is regulated by means of a heat exchanger equipped with a solenoid valve and a PID controller fed by the signal provided by a resistance thermometer (RTD) located at the outlet of the test duct, and then it is raised by means of an electric heater located downstream of the pump; the heat supply is controlled with a second PID using as input signal the temperature given by an RTD located just upstream of the test duct. Additionally, PMA P40 and Kistler K-line piezoresistive silicon pressure sensors were used to determine the pressure drop across the test duct.

In the second circuit (bottom of Fig. 1.), thermal oil is used as the heating fluid for the test duct. This heating circuit had previously been used and validated for other applications (Torregrosa *et al.* 2010; Serrano *et al.* 2010), and comprises an expansion tank, an electric oil pump, temperature and pressure control systems and several valves for mass flow rate control. Heat is supplied by an electrical heater with three electrical resistances (total nominal power of 37.5 kW). The thermal oil delivered by the system can reach temperatures up to 300 °C with volumetric flow rates up to 6.5 m^3/h. The oil temperature at the system outlet is controlled by a PID that switches on or off the resistors available. The flow rate is controlled by manually adjusting the valves until the prescribed value of the oil mass flow is achieved.

The test section is a horizontal rectangular duct 1000 mm long, 52 mm wide and 52 mm high, built in extruded 6062T6 anodized aluminum. The heating section is 40 mm wide and 300 mm long, and is located 550 mm away from the inlet, i.e. more than 10 hydraulic diameters from the inlet, so that one should expect the flow to be substantially developed. In the configuration used, only part of the fluid circulating within the duct is in contact with the heater surface and reaches the saturation temperature. The measurement section is shown schematically in Fig. 2., where it can be seen that the test duct is equipped with a window to allow observation of bubble growth and evolution. The window was constructed of polycarbonate with

a thermal conductivity $k = 0.22\ \mathrm{Wm^{-1}K^{-1}}$, and thus some small heat losses to the surroundings are implied by its use. Additionally, since the integrity of the polycarbonate window is compromised for temperatures above 160 °C, the maximum test temperature was kept below that value.

As also shown in Fig. 2., the heater surface temperature was measured with six K-type thermocouples inserted to a depth of 1 mm in the heating block and arranged in three sections. The heating block consists of a piece of aluminum with a cylindrical bore in its center, through which the hot thermal oil circulates. Heat transfer takes place by convection from the hot oil to the heating block, by conduction up to the block surface and again by convection or boiling from the heater surface to the coolant. Uncertainties in measured parameters associated with the stability provided by the set-up control and the sensitivity of the sensors used are shown in Table 1.

Table 1 Measured parameters and their uncertainties

Parameter	Uncertainty (%)
Temperature (°C)	±1
Pressure (Pa)	±0.4
Coolant flow rate (kg s^{-1})	±0.5

As also indicated in Fig. 2., the acquisition of experimental data on bubble diameters was performed through optical techniques. A Sensicam PCO high speed camera with a resolution of 1276×1040 pixels and with a capacity of 10 images per second was used, together with a 300 W white light source. Shots were triggered with a TTI TG210 signal generator with a frequency range from 0.2 Hz to 2 MHz. It should be noticed that, with the experimental arrangement considered (most notably, without back-lighting) and the instrumentation available (in particular, the acquisition frequency of the high-speed camera) it is not possible to determine the actual lift-off radius of the bubbles, but only its evolution once the bubble detaches from the heater surface.

As an example of the images acquired, in Fig. 3. the trajectory of a bubble has been reconstructed from the superposition of four successive images. It is possible to observe that, within the accuracy associated with the spatial resolution of the images, the bubble radius does not change in a significant manner, so that one should expect that the observed radius does not differ significantly from the lift-off radius, and thus that the data collected may allow not only for the study of the radius distribution, but also for

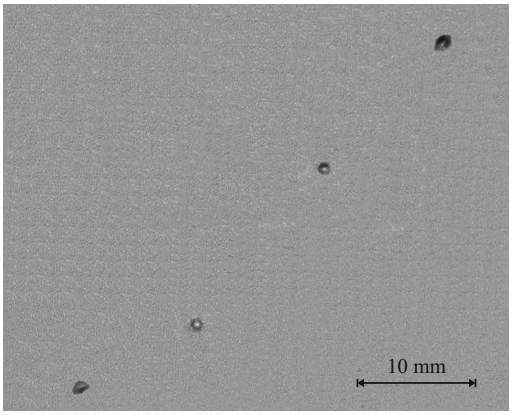

Fig. 3. Reconstruction of a bubble trajectory from the combination of four consecutive images.

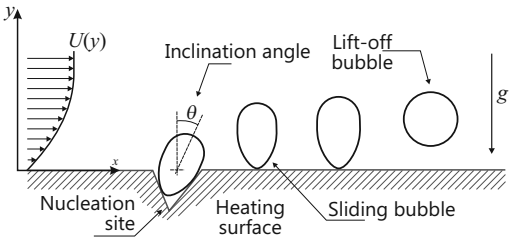

Fig. 4. Schematic representation of bubble formation, sliding and detachment.

checking the possibility of using mechanistic models for the interpretation of the mean results obtained.

A sample of the material used to build the test duct was used for the characterization of the heater surface roughness. This was performed with a Mahr M2 Perthometer, with a measuring range of up to 150 μm, phase-correct profile filter as per ISO 11562 and a cutoff of 0.25 mm. The roughness distribution was obtained with an Agilent G-200 nanoindenter with a Berkovich-type pyramidal tip. A $100\mu\mathrm{m}\times100\mu\mathrm{m}$ sweep on the surface of the sample was performed; a load of 6μN was applied in the tip in order to keep it in contact with the surface.

3. MECHANISTIC MODEL

The starting point for the estimation of the size of the bubbles was the evolution model proposed by Zeng *et al.* (1993). This model assumes that the process of detachment of the bubbles takes place in three phases: first, the bubble is anchored at a nucleation site, with an inclination to the vertical θ due to the hydrodynamic drag forces acting on it (see Fig. 4., adapted from (Zeng *et al.* 1993)). Then, the bubble grows until it reaches a certain critical

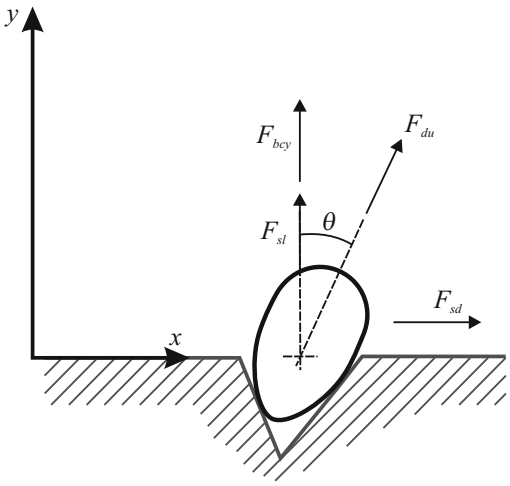

Fig. 5. Forces acting on a bubble at the time of detachment.

volume, when it departs the nucleation site, so that the second phase starts, in which the bubble slides in contact with the wall and in upright position($\theta = 0$), continuing to grow until it reaches a volume such that the buoyancy forces are sufficiently strong so that the bubble is separated from the wall.

The different forces acting on the bubble are represented in Fig. 5.: F_{sd} is the quasi-steady drag force, F_{sl} is the lift force associated with the shear stress on the wall, F_{bcy} is the buoyancy force and F_{du} is the unsteady drag force associated with the asymmetrical growth of the bubble. The steady drag force is given by:

$$F_{sd} = 6C_d \pi \mu_f u r \tag{1}$$

where

$$C_d = [(12/\mathrm{Re}_b)^n + 0.796^n]^{-1/n} + 2/3$$

with $n = 0.65$, whereas the shear lift force can be expressed as

$$F_{sl} = C_{sl} \rho_f u^2 \pi r^2/2 \tag{2}$$

where the shear lift coefficient C_{sl} is given by

$$C_{sl} = 3.877 G_s^{1/2} \left(\mathrm{Re}_b^{-2} + 0.014 G_s^2\right)^{1/4} \tag{3}$$

In equations (1) and (2) u represents the velocity of the bubble relative to the flow, r is the bubble radius, and the bubble Reynolds number Re_b and the dimensionless velocity gradient G_s are expressed as:

$$\mathrm{Re}_b = \rho_f u 2r/\mu_f \ , \ G_s = |\mathrm{d}U/\mathrm{d}y|_{y=r}\, r/u \tag{4}$$

where y is the coordinate perpendicular to the wall. To estimate the relative velocity profile near the wall it is assumed that the presence of the bubbles can be neglected, and therefore Reichardt's single-phase expression for turbulent flow can be used:

$$u^+ = U/u_\tau = \ln(1+\kappa y^+)/\kappa + \xi(y^+) \tag{5}$$

with

$$\xi(y^+) = c\left(1 - \mathrm{e}^{-y^+/\chi} - (y^+/\chi)\mathrm{e}^{-y^+/3}\right)$$

being the values of the tuning constants $\kappa = 0.41$, $\chi = 11$ and $c = 7.4$. The non-dimensional coordinate y^+ is defined as

$$y^+ = \rho_f u_\tau y/\mu_f \tag{6}$$

where the friction velocity at the wall u_τ is given by

$$u_\tau = (\tau_w/\rho_f)^{1/2} \tag{7}$$

that is determined by the shear stress at the wall, which in turn can be written in terms of the friction factor ζ as

$$\tau_w = (\zeta/4)\rho_f (U_f^2/2) \tag{8}$$

where U_f is the area-averaged fluid velocity. It is thus clear that some estimate of the surface roughness is required for assessing the shear stress at the wall. According to pool boiling studies (Benjamin and Balakrishnan 1996) the surface roughness can be obtained from a literature correlation in the micro-roughness range, but here its direct determination was preferred.

Regarding the relative velocity of the bubble, following Situ *et al.* (2005) a relative velocity coefficient was defined as

$$C_r = u/U \tag{9}$$

so that $C_r = 1$ when the bubble is not sliding, and zero when the bubble velocity is the same as that of the fluid. Then, from equations (4) and (5) one gets

$$G_s = |u_\tau/\kappa y|\, r/u = (C_r \kappa u^+)^{-1} \tag{10}$$

Finally, the buoyancy force is given by

$$F_{bcy} = (4/3) r^3 \pi g (\rho_f - \rho_g) \tag{11}$$

and the force associated with bubble growth can be computed as (Zeng *et al.* 1993)

$$F_{du} = -\rho_f \pi r^2 \left((3/2)C_s \dot{r}^2 + r\ddot{r}\right) \tag{12}$$

where C_s is an empirical constant that accounts for the effects of the presence of the wall and whose value was suggested to be set to 20/3. The use of equation (12) requires the determination of the temporal evolution of the bubble radius and its derivatives, but there is not a general agreement on the expression to be used. Zeng *et al.* (1993) adopted a diffusion-controlled model proposed by Zuber (1961), according to which

$$r(t) = 2b\mathrm{Ja}(\alpha_f/\pi)^{1/2} t^{1/2} \equiv G_b t^{1/2} \tag{13}$$

where b is an empirical constant that accounts for asphericity, α_f is the thermal diffusivity of the liquid, t is the time and Ja is the Jacob number, defined as

$$\mathrm{Ja} = \rho_f c_{p,f}(T_w - T_s)/(\rho_g l_{fg}) \tag{14}$$

Here, $c_{p,f}$ is the liquid specific heat and l_{fg} is the latent heat of vaporization. Two main issues can be pointed out regarding equation (13): the value of the constant b and the exponent of t. While originally b was supposed to take values between 1 and 1.73, depending on the flow conditions and the characteristic of the nucleation site, Steiner *et al.* (2005) obtained the best fit to their measurements in water with $b = 0.21$, whereas Cho *et al.* (2011) reported values ranging from 0.48 to 24.24 depending on the working fluid, the pressure, the wall superheat, etc. With respect to the time exponent, Thorncroft *et al.* (1998) found that $r \propto t^n$ with n between 1/3 and 1/2, whereas Chen *et al.* (2010) reported a value of about 1/4.

At the time of bubble departure, the inertial terms are assumed to be negligible (which is justified since the density of the vapor phase is much smaller than that of the liquid) and so is the surface tension, given that the pressure is not too high (Wu *et al.* 2008). Therefore, the balance of forces reads:

$$0 = F_{sd} + F_{du}\sin\theta \tag{15}$$

$$0 = F_{bcy} + F_{du}\cos\theta + F_{sl} \tag{16}$$

Substitution of equations (1), (2), (11) (12) and (13) into equations (15) and (16) gives

$$6C_d\mu_f u r_d - \rho_f G_b^4 \tilde{C}_s \sin\theta = 0 \tag{17}$$

$$\frac{4}{3}\rho^* g r_d^3 + \frac{1}{2}C_{sl} u r_d^2 - G_b^4 \tilde{C}_s \cos\theta = 0 \tag{18}$$

where $\rho^* = (\rho_f - \rho_g)/\rho_f$ and $\tilde{C}_s = 3C_s/8 - 1/4$. The simultaneous solution of equations (17) and (18) provides both the departure radius r_d and the inclination angle θ.

The lift-off radius is then determined by assuming that there is no velocity slip between the bubble and the surrounding liquid, so that the drag and shear lift forces vanish and the bubble is in the upright position ($\theta = 0$), thus giving

$$0 = F_{bcy} + F_{du} \tag{19}$$

which, making use of equations (11) and (12) can be written in terms of the bubble radius as

$$((4/3)\rho^* g - \ddot{r})\, r = (3/2)C_s \dot{r}^2 \tag{20}$$

Now, as suggested by Cho *et al.* (2011), the bubble growth model defined by equation (13) is modified so that the point of bubble departure is explicitly expressed, as

$$r(t) = r_d + G_{bd}(t - t_d)^{1/2} \tag{21}$$

where t_d is the departure time, and $G_{bd} = 2b_d\mathrm{Ja}(\alpha_f/\pi)^{1/2}$, being b_d the growth constant after departure, which in general should be smaller than the growth constant b before departure, since the contact diameter decreases after the bubble departure (Cho *et al.* 2011). Now, the lift-off radius can be expressed in terms of the sliding time $t_{sld} = t_{lo} - t_d$, i.e. the difference between the departure time and the lift-off time t_{lo}, as

$$r_{lo} = r_d + G_{bd} t_{sld}^{1/2} \tag{22}$$

Then, at the point of bubble lift-off, equation (20) can be written as

$$\left(\frac{4}{3}\rho^* g + \frac{1}{4}G_{bd} t_{sld}^{-3/2}\right) r_{lo} = \frac{3}{8}C_s G_{bd}^2 t_{sld}^{-1} \tag{23}$$

Finally, introducing the non-dimensional ratios

$$r^* = \frac{r_{lo} - r_d}{r_d} = \frac{G_{bd} t_{sld}^{1/2}}{r_d}\,;\, \varphi = \frac{3G_{bd}^4}{16\rho^* g r_d^3} \tag{24}$$

equation (23) can be written as

$$1 + r^* + \frac{1}{r^{*3}}\varphi + \frac{1}{r^{*2}}\varphi\left(1 - \frac{3}{2}C_s\right) = 0 \tag{25}$$

In this way, the problem is closed and it is possible to relate the lift-off radius with the corresponding departure radius, given that the empirical constant b_d is known. This could be obtained in principle if data for both r_{lo} and r_d were available, so that equation (25) could be solved for φ and then G_{bd} and thus b_d would be obtained. However, in the present investigation only values of r_{lo} could be experimentally estimated, and the values for r_d provided by equations (17) and (18) are affected by substantial uncertainties and cannot be fully relied on without some experimental evidence on the actual values of r_d. In order to obtain such evidence without the direct determination of r_d, an alternative approach was attempted that is described next.

In previous work by the authors (Torregrosa *et al.* 2014) it was verified that the heat fluxes measured in the present experimental configuration are well represented by a Chen-type correlation (Chen 1966) so that the total heat flux is written as the addition of a purely convective component q_{fc} and a nucleate boiling component q_{nb}:

$$q_w = q_{fc} + q_{nb} \tag{26}$$

The nucleate boiling heat flux q_{nb} is given by

$$q_{nb} = Sh_{nb}(T_w - T_s) \tag{27}$$

where T_s is the saturation temperature and the correlation proposed by Forster and Zuber (1955) for pool boiling heat transfer was used to compute the heat transfer coefficient h_{nb}, whereas the suppression factor S accounts for the decrease in nucleate boiling activity observed when the flow velocity increases. It was found that, in the present experimental conditions, the suppression factor can be satisfactorily represented by (Torregrosa *et al.* 2014)

$$S = \psi\left(1 + 2.53\times10^{-6}\mathrm{Re}_{2\phi}^{1.17}\right)^{-1} \tag{28}$$

where $\mathrm{Re}_{2\phi}$ is the two-phase Reynolds number and ψ depends only on the Prandtl number. Now, Steiner *et al.* (2005) noted that with increasing flow rate there is a noticeable decrease of the the departure radius r_d relative to the lift-off radius r_{lo}, the difference observed being wider as the bulk velocity increases, reflecting the influence of the local velocity field on bubble detachment. Based on this consideration they suggested that the suppression factor can be written as

$$S = r_d / r_{lo} \tag{29}$$

It should be noticed, however, that in this way S actually represents the flow-induced deviation of the bubble departure radius from the corresponding pool boiling limit, so that r_{lo} basically represents the lift-off radius in the saturated boiling regime. Equations (28) and (29) provide thus the required link with the present measurements, allowing for the estimation of b_d. By substituting equation (29) into equation (24), one gets $r^* = S^{-1} - 1$, and then from equation (25) one has

$$\varphi = -\frac{(1-S)^2}{S^3}\left[\frac{S}{1-S} + 1 - \frac{3}{2}C_s\right]^{-1} \tag{30}$$

From equations (21) and (24) it is then possible to obtain the value of b_d. Now, the other major uncertainty associated with the determination of the departure radius was the value of empirical growth rate parameter b, but this issue can also be addressed by assuming that equation (29) holds. Effectively, setting $r = Sr_{lo}$, equations (17) and (18) may be solved for G_b and θ, thus providing an estimate of b and completing the model.

4. RESULTS AND DISCUSSION

4.1 Experimental Plan

Experimental tests were carried out in order to obtain a representative data set covering a significant range of engine-like operating conditions. Measurements were performed with a mixture of 50% water and 50% ethylene glycol (volume percentages). Values of 1 $\mathrm{m^3h^{-1}}$, 1.5 $\mathrm{m^3h^{-1}}$ and 2 $\mathrm{m^3h^{-1}}$ were considered for the coolant flow, whereas a value of 90 °C was chosen for the coolant temperature at the inlet of the heating circuit. The temperature of the thermal oil was varied between 100 °C and 280 °C at increments of 40 °C, while keeping its flow rate constant at 1.92 $\mathrm{m^3h^{-1}}$.

With the chosen duct configuration, coolant fluid velocities within the range 0.1 $\mathrm{ms^{-1}} \leq U_f \leq 0.2$ $\mathrm{ms^{-1}}$ with Reynolds numbers ranging from 4300 to 8500 could be achieved. The operating pressure was within the range $1.5 \leq p \leq 1.9$ bar. Table 2 summarizes the values of the relevant magnitudes in all the experiments.

Table 2 Experimental matrix considered

p (bar)	$\dot{V}$ ($\mathrm{m^3h^{-1}}$)	U_f (m/s)	T_s (°C)
1.9	1.0	0.10	126.1
1.5	1.5	0.15	127.0
1.6	2.0	0.20	126.9

4.2 Image Processing

In order to determine the dimensions of the bubbles observed, digital image processing was used. The main purpose was to enhance the quality of the raw images acquired with the high speed camera, most notably regarding its contrast. Numerous algorithms are available with this purpose, and the choice of one or another is still an object of research. Here, the classical approach based on punctual (pixel-to-pixel) operations was used (Pratt 2007). The first step of the procedure used was the contrast enhancement, followed by a median filter for the removal of spurious spots. Then, two fundamental morphological operations (image erosion and dilatation) were used and finally a Laplace operator was applied in order to obtain the contour of the bubbles. Once the contours were detected, the number of pixels intercepted was determined and then an equivalent bubble radius was estimated.

4.3 Surface Characterization

The surface parameters determined for the heater surface are shown in Table 3 (see for instance Gadelmawlaa *et al.* (2002) for the precise definitions of those parameters and their interpretation).

Table 3 Roughness parameters

Arithmetic average height (R_a)	0.160 μm
Root mean square roughness (R_q)	0.224 μm
Maximum height of peaks (R_p)	1.84 μm
Maximum height of the profile (R_t)	2.04 μm
Ten-point height (DIN) (R_z)	1.28 μm

The values obtained for the surface parameters suggest a high irregularity in the surface characteristics; in particular, this is indicated by the fact that $R_q > R_a$, and by the comparatively high values of R_p, R_t and R_z, which are specially sensitive to occasional high peaks or deep valleys or scratches (Gadelmawlaa *et al.* 2002).

Note that the average roughness R_a in cooling galleries of reciprocating internal combustion engines is of the order of 40 μm (Steiner *et al.* 2011), which is large compared to the values found in this experiment. Thus, the surfaces of usual cooling galleries would produce bubbles with departure diameters larger than those observed with low surface roughness, apart from the reported effect on the heat transfer itself (Wu *et al.* 2008; Ramstorfer *et al.* 2008).

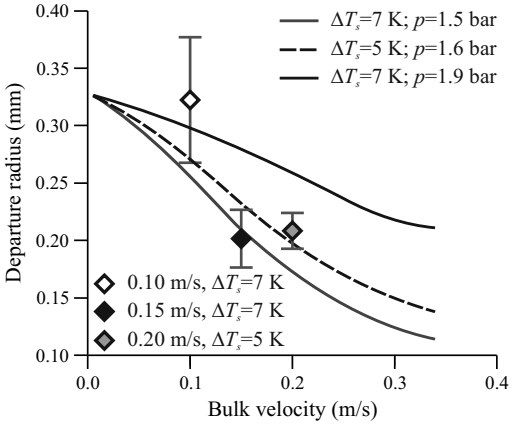

Fig. 6. Comparison of measured and modeled results for the dependence of bubble departure radius on flow velocity for different wall superheats and fluid pressures.

4.4 Discussion of Results

The procedure described in section 3 was applied to the particular conditions of the experiment, and a value of 0.527 was obtained for the growth rate constant b. Then, by solving the model equations the dependency of the departure radius on the bulk flow velocity was obtained. Such dependence is shown in Fig. 6., where it can be observed that the trend obtained is that expectable, considering for instance the results shown by Steiner *et al.* (2005). Additionally, the model appears to be sensitive to the wall superheat ΔT_s and to the fluid pressure (Yuan *et al.* 2011), as suggested by the role of the Jacob number in the bubble growth model.

In order to check the actual applicability of the model to the flow conditions considered, from the bubble diameters obtained from the digital processing of the photographic images, the corresponding departure radii were estimated making use of equations (28) and (29). The mean and the population standard deviation were identified for each flow condition considered. The results have also been plotted in Fig. 6., where it can be observed that, in general, reasonable agreement between the measured points and the corresponding model is obtained. The agreement is somehow poorer in the case of the smallest velocity and highest fluid pressure, which according to Wu *et al.* (2008) could be due to the omission of surface tension in the balance of forces. The predicted tendencies are thus consistent with the present experimental results, even if the lack of a parametric variation of the flow velocity does not allow for a full validation of the model.

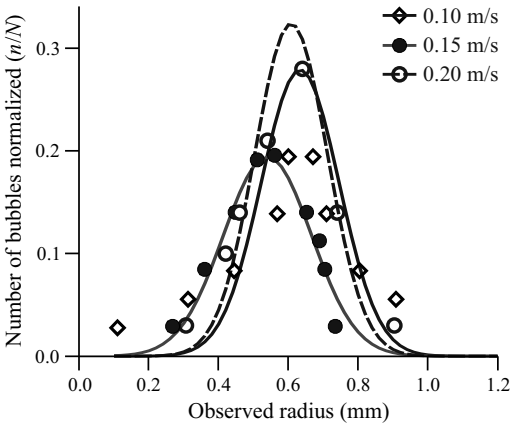

Fig. 7. Measured distribution of bubble radius and fit to a normal distribution.

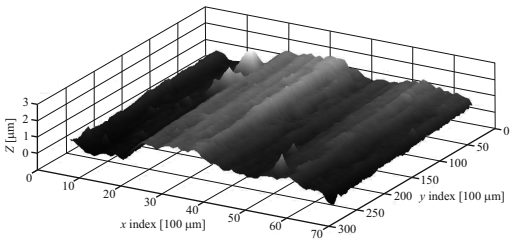

Fig. 8. Topographic image of the heater surface.

Therefore, one may assume that a suitable estimate of departure and lift-off radii can be achieved by the use of the model. Apart from this aspect, it is clear that it would also be necessary to supplement the model with some estimate of the expected dispersion in the radii distribution, in view of the remarkable scatter found in the measurements. In order to explore this possibility, a study of the probability distribution that may better represent the experimental data was performed, along the lines indicated by Klausner *et al.* (1997).

It is well known that evaporation is a stochastic process. The work of Klausner *et al.* (1997) starts on the well-established premise that increasing the average temperature of the heating zone produces an increase in the size of the bubbles, and that when increasing the mean fluid velocity the diameter of the vapor bubbles tends to decrease, as predicted by the model of Zeng *et al.* (1993) and confirmed by the present work. Klausner *et al.* (1997) consistently found that both the mean and the standard deviation of the distributions increased with the overheating considered (i.e. the difference between wall temperature and the corresponding saturation temperature). This simple dependence allows writing the distribution of radii in terms of the distribution of overheatings as (Klausner *et al.* 1997)

$$P(r) = P_{\Delta T}(\Delta T)\,|\delta\Delta T/\delta r| \tag{31}$$

where the derivative can be estimated from the model equations described in Section 3 and, in the absence of any alternative approach or some additional experimental evidence, it is assumed that the distribution of overheating follows a Gaussian profile such as

$$P_{\Delta T}(\Delta T) = \frac{1}{\sigma_{\Delta T}\sqrt{2\pi}} \exp\left[-\frac{1}{2}\left(\frac{\Delta T - \Delta T_m}{\sigma_{\Delta T}}\right)^2\right] \tag{32}$$

where ΔT_m is the mean overheating over the heating surface and $\sigma_{\Delta T}$ is the corresponding standard deviation. For similar reasons, a Gaussian profile was also assumed for the velocity fluctuations.

The results of the present experiment are shown in Fig. 7., along with the corresponding normal distribution functions for the three velocity conditions tested (0.1 ms^{-1}, 0.15 ms^{-1} and 0.2 ms^{-1}). The results showed a correlation coefficient of 94 % with such a probability distribution function. However, even if the results are overall comparable to those shown by Zeng *et al.* (1993), Klausner *et al.* (1997) and Mei *et al.* (1995), it appears that a significant number of the experimental points are not fully consistent with that distribution function. This may be due to the fact that the fluid used (in this case a 50 % in volume mixture of water and ethylene glycol) is different from that used in those experiments, apart that different pressures (between 1.82 and 2 bar) were considered.

In order to get further insight into this issue, from the surface characterization of the heating surface, the topographic image of the material shown in Fig. 8. was obtained. With the purpose to obtain information about the size distribution of potential nucleation sites, first the surface features related with the fabrication process were removed by subtracting the average surface profile along the x direction, so that a flat projection of the surface was obtained. In the resulting surface a suitable small threshold below the average level was set that allowed the identification of small low level cavities likely to be potential nucleation sites, according to Wu *et al.* (2008) and Kandlikar and Stumm (1995). The resulting data matrix was then transformed into a binary image, from which the size of the

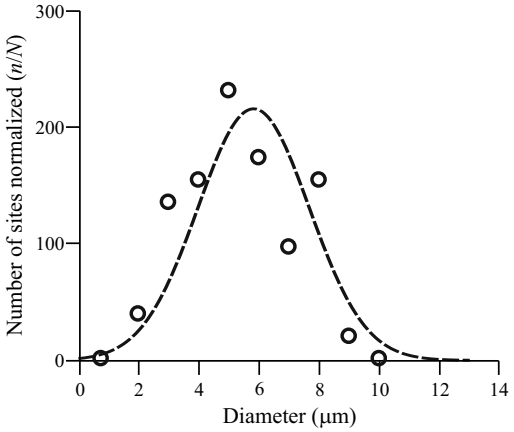

Fig. 9. Size distribution of potential nucleation sites and fit to a normal distribution.

sites was estimated in a similar way as that previously used for bubble size estimation.

The resulting distribution of sizes of potential nucleation sites is shown in Fig. 9., together with the results of fitting it to a normal distribution. It appears that also in this case, even if the correlation coefficient is again 94%, the distribution could be better represented by a different probability function. However, while this could indicate that there is a certain relationship between the size distribution of the potential nucleation sites and that of the detached bubbles, the results are not sufficiently conclusive, all the more if the stochastic nature of bubble formation and growth are taken into account. In fact, Wu *et al.* (2008) reported that in their experiments the bubble contact diameter before bubble departure remained nearly a constant regardless of increasing bubble size.

As a byproduct of this surface analysis, additional evidence on the consistency of the observed bubble sizes can be obtained. According to Wu *et al.* (2008), the bubble contact diameter is directly related to the size of the nucleation site. In this sense, the mean value of $\sim 6\mu$m obtained in this work is rather consistent with the departure radii estimated: assuming that the bubbles are approximately spherical before departure, and estimating the depth of the nucleation cavity to be of the order of magnitude of the surface roughness, a value of $\sim 250\mu$m is obtained for the departure radius, which lies within the range found in the present experiments, as can be seen from Fig. 6.

5. CONCLUSIONS

Experiments on subcooled boiling flow in temperature conditions similar to those occurring in cooling jackets of internal combustion engines were performed. The study was focused on the low velocity range, as such values may by locally present in some engine cooling passages as a consequence of the use of advanced thermal management strategies, and there appears to be little experimental evidence for this case.

An experimental rig allowing for the control of the coolant flow and the temperature was built, and measurements were taken at a representative inlet temperature and three coolant velocities. A high-speed photographic camera was used to collect images of the detached vapor bubbles. Also, the microscopic characteristics of the heating surface were studied in order to check the plausibility of the results and to analyze the eventual relation between the surface characteristics and the resulting distribution of bubble sizes.

A standard model for the prediction of departure and lift-off radii was implemented in order to check its ability to reproduce the behavior observed in the present experimental conditions. Only detached bubble radii were obtained from the experiments, but the observed evolution suggested that the observed radii provided an acceptable estimate of the lift-off radii. Then, in order to determine the values of the empirical bubble growth constants it was assumed that the ratio of the departure to the lift-off diameter is precisely the suppression factor. With this assumption, the model provided acceptable results for the average radius under different velocities, wall superheats and fluid pressures, showing consistent trends under changes in these conditions.

Finally, the possibility to complement the picture provided by the model with some estimate of the size distribution was studied. The statistical evaluation of the data of bubble diameters, showed a correlation coefficient of 94% when assuming a normal probability function, but a significant number of experimental points were left outside of the distribution. Therefore, a statistical analysis of the size distribution of potential nucleation sites was performed, but the results cannot be considered conclusive of a direct relation between both distributions. However, the analysis of the surface structure provided additional evidence on the consistency of the results obtained.

ACKNOWLEDGMENTS

The equipment used in this work has been partially supported by FEDER project funds "Dotación de infraestructuras científico técnicas

para el Centro Integral de Mejora Energética y Medioambiental de Sistemas de Transporte (CiMeT), (FEDER-ICTS-2012-06)", framed in the operational program of unique scientific and technical infrastructure of the Ministry of Science and Innovation of Spain. O. Cornejo is indebted to Senacyt Panamá for their support. The authors wish to thank Dr. D. Busquets and Dr. E. Rayón their kind cooperation in the surface characterization and in the interpretation of its results.

REFERENCES

Ajotikar, N., B. J. Eggart and S. A. Miers (2010). Nucleate boiling identification and utilization for improved internal combustion engine efficiency. In *Proc. ASME Internal Combustion Engine Division Fall Technical Conference* 949–958.

Benjamin, R. J. and A. R. Balakrishnan (1996). Nucleate pool boiling heat transfer of pure liquids at low to moderate heat fluxes. *Int. J. Heat Mass Transfer 39(12),* 2495–2504.

Campbell, N. A. F. and J. G. Hawley (2003). Predicting Critical Heat Flux as a precursor to a boiling-based IC engine-cooling strategy. *Journal Of The Institute Of Energy 76(506),* 22–28.

Campbell, N. A. F., D. G. Tilley, S. A. MacGregor and L. Wong (1997). Incorporating nucleate boiling in a precision cooling strategy for combustion engines. *SAE Paper 971791*.

Chen, D. Q., L. M. Pan and S. Ren (2012). Prediction of bubble detachment diameter in flow boiling based on force analysis. *Nucl. Eng. Des. 243,* 263–271.

Chen, D. Q., L. M. Pan, D. Yuan and X. J. Wang (2010). Dual model of bubble growth in vertical rectangular narrow channel. *Int. Commun. Heat Mass Transfer 37(8),* 1004–1007.

Chen, J. C. (1966). Correlation for boiling heat transfer to saturated fluids in convective flow. *I&EC Process Des. Dev. 5(3),* 322–329.

Cho, Y. J., S. B. Yum, J. H. Lee and G. C. Park (2011). Development of bubble departure and lift-off diameter models in low heat flux and low flow velocity conditions. *Int. J. Heat Mass Transfer. 54(15-16),* 3234–3244.

Finlay, I. C., D. Harris, D. J. Boam and B. I. Parks (1985). Factors influencing combustion chamber wall temperatures in a liquid cooled, automotive spark ignition engine. *Proc. Inst. Mech. Eng., Part D 199(3),* 207–214.

Forster, H. K. and N. Zuber (1955). Dynamics of vapor bubbles and boiling heat transfer. *AIChE J. 1*(4) 531–535.

Gadelmawlaa, E. S., M. M. Kourab, T. M. A. Maksoudc, I. M. Elewaa and H. H. Solimand (2002). Roughness parameters. *J. Mater. Process. Technol. 123(1),* 133–145.

Hamzekhani, S., M. Maniavi-Falahieh, M. R. Kamalizadeh and M. Salmaninejad (2015). Bubble dynamics for nucleate pool boiling of water, ethanol and methanol pure liquids under the atmospheric pressure. *J. Appl. Fluid Mech. 8(4),* 893–898.

Kandlikar, S. G. and B. J. Stumm (1995). A control volume approach for investigating forces on a departing bubble under subcooled flow boiling. *J. Heat Transfer 117(4),* 990–997.

Klausner, J. F., R. Mei and L. Z. Zeng (1997). Predicting stochastic features of vapor bubble detachment in flow boiling. *Int. J. Heat Mass Transfer 40(15),* 3547–3552.

Knecht, W. (2008). Diesel engine development in view of reduced emission standards. *Energy 33(2),* 264–271.

Lee, H., S. Li, Y. Hwang, R. Radermacher and H. H. Chun (2013). Experimental investigations on flow boiling heat transfer in plate heat exchanger at low mass flux condition. *Appl. Therm. Eng. 61(2),* 408–415.

Mei, R., W. C. Chen and J. F. Klausner (1995). Vapor bubble-growth in heterogeneous boiling. 1. Formulation. *Int. J. Heat Mass Transfer 38(5),* 909–919.

Pang, H. H. and C. J. Brace (2004). Review of engine cooling technologies for modern engines. *Proc. Inst. Mech. Eng., Part D 218(11),* 1209–1215.

Pratt, W. K. (2007). *Digital Image Processing* (4th ed.) Wiley.

Ramstorfer, F., H. Steiner, G. Brenn, C. Kormann and F. Rammer (2008). Subcooled boiling flow heat transfer from plain and enhanced surfaces in automotive applications. *J. Heat Transfer 130(1),* 011501.

Robinson, K., N. A. F. Campbell, J. G. Hawley and D. G. Tilley (1999). A review

of precision engine cooling. *SAE Paper* 1999-01-0578.

Sarafraz, M. M. (2013). Experimental investigation on pool boiling heat transfer to formic acid, propanol and 2-butanol pure liquids under the atmospheric pressure. *J. Appl. Fluid Mech. 6(1),* 73–79.

Serrano, J. R., P. Olmeda, A. Páez and F. Vidal (2010). An experimental procedure to determine heat transfer properties of turbochargers. *Meas. Sci. Technol. 21(3),* 035109.

Sher, E. and I. Sher (2011). Theoretical limits of scaling-down internal combustion engines. *Chemical Engineering Science 66(3),* 260–267.

Singh, O. P., M. Garg, V. Kumar and Y. V. Chaudhary (2013). Effect of cooling system design on engine oil temperature. *J. Appl. Fluid Mech. 6(1),* 61–71.

Situ, R., T. Hibiki, M. Ishii and M. Mori (2005). Bubble lift-off size in forced convective subcooled boiling flow. *Int. J. Heat Mass Transfer 48(25-26),* 5536–5548.

Situ, R., M. Ishii, T. Hibiki, J. Tu, G. Yeoh and M. Mori (2008). Bubble departure frequency in forced convective subcooled boiling flow. *Int. J. Heat Mass Transfer 51(25-26),* 6268–6282.

Steiner, H., G. Brenn, F. Ramstorfer and B. Breitschädel (2011). Increased cooling power with nucleate boiling flow in automotive engine applications. In M. Chiaberge (Ed.), *New trends and developments in automotive system engineering,* Chapter 13, 249– 272. In Tech.

Steiner, H., A. Kobor and L. Gebhard (2005). A wall heat transfer model for subcooled boiling flow. *Int. J. Heat Mass Transfer 48*(19-20), 4161–4173.

Taylor, A. M. K. P. (2008). Science review of internal combustion engines. *Energy Policy 36(2),* 4657–4667.

Thorncroft, G. E., J. F. Klausner and R. Mei (1998). An experimental investigation of bubble growth and detachment in vertical upflow and downflow boiling. *Int. J. Heat Mass Transfer 41(23),* 3857–3871.

Torregrosa, A. J., A. Broatch, P. Olmeda, and O. Cornejo (2014). Experiments on subcooled flow boiling in i.c. engine-like conditions at low flow velocities. *Exp. Therm. Fluid Sci. 52,* 347-354.

Torregrosa, A. J., A. Broatch, P. Olmeda and J. Martín (2010). A contribution to film coefficient estimation in piston cooling galleries. *Exp. Therm. Fluid Sci. 34(2),* 142151.

Torregrosa, A. J., A. Broatch, P. Olmeda and C. Romero (2008). Assessment of the influence of different cooling system configurations on engine warm-up, emissions and fuel consumption. *Int. J. Automot. Technol. 9(4),* 447–458.

Torregrosa, A. J., P. Olmeda, A. Gil and O. Cornejo (2015). Computational fluid dynamics assessment of subcooled flow boiling in internal-combustion engine-like conditions at low flow velocities with a volume-of-fluid model and a two-fluid model. *Proc. Inst. Mech. Eng., Part D 229(13),* 1830–1839.

Torregrosa, A. J., P. Olmeda, J. Martín and B. Degraeuwe (2006). Experiments on the influence of inlet charge and coolant temperature on performance and emissions of a DI Diesel engine. *Exp. Therm. Fluid Sci. 30(7),* 633-641.

Tu, J. Y. and G. H. Yeoh (2002). On numerical modelling of low-pressure subcooled boiling flows. *Int. J. Heat Mass Transfer 45(6),* 1197–1209.

Wu, W., and P. Chen and B. G. Jones (2008). A study on bubble detachment and the impact of heated surface structure in subcooled nucleate boiling flows. *Nucl. Eng. Des. 238,* 2693–2698.

Yuan, D., L. M. Pan, D. Q. Chen, H. Zhang, J. H. Wei and Y. P. Huang (2011). Bubble behavior of high subcooling flow boiling at different system pressure in vertical narrow channel. *Appl. Therm. Eng. 31(16),* 3512–3520.

Zeng, L. Z., J. F. Klausner, D. M. Bernhard and R. Mei (1993). A unified model for the prediction of bubble detachment diameters in boiling systems. 2. Flow boiling. *Int. J. Heat Mass Transfer 36(9),* 2271–2279.

Zuber, N. (1961). The dynamics of vapor bubbles in nonuniform temperature fields. *Int. J. Heat Mass Transfer 2(1-2),* 83–98.